

Traveling length and minimal traveling time for flow through percolation networks with long-range spatial correlations

A. D. Araújo,^{1,2} A. A. Moreira,¹ H. A. Makse,³ H. E. Stanley,⁴ and J. S. Andrade Jr.¹

¹Departamento de Física, Universidade Federal do Ceará, 60451-970 Fortaleza, Ceará, Brazil.

²Departamento de Física, Universidade Vale do Acaraú, 62040-370 Sobral, Ceará, Brazil.

³Department of Physics, City College of New York, New York 10031-9198, USA.

⁴Center for Polymer Studies and Department of Physics,

Boston University, Boston, Massachusetts 02215, USA.

(Dated: 20 April 2002)

We study the distributions of traveling length l and minimal traveling time t_{min} through two-dimensional percolation porous media characterized by long-range spatial correlations. We model the dynamics of fluid displacement by the convective movement of tracer particles driven by a pressure difference between two fixed sites (“wells”) separated by Euclidean distance r . For strongly correlated pore networks at criticality, we find that the probability distribution functions $P(l)$ and $P(t_{min})$ follow the same scaling *Ansatz* originally proposed for the uncorrelated case, but with quite different scaling exponents. We relate these changes in dynamical behavior to the main morphological difference between correlated and uncorrelated clusters, namely, the compactness of their backbones. Our simulations reveal that the dynamical scaling exponents d_l and d_t for correlated geometries take values intermediate between the uncorrelated and homogeneous limiting cases, where $l^* \sim r^{d_l}$ and $t_{min}^* \sim r^{d_t}$, and l^* and t_{min}^* are the most probable values of l and t_{min} , respectively.

PACS numbers: 47.55.Mh, 64.60.Ak

I. INTRODUCTION

Fluid transport in porous media is of central importance to problems in petroleum exploration and production [1, 2, 3, 4]. The geometry of an oil field can be very complex, displaying heterogeneities over a wide range of length scales from centimeters to kilometers [5]. The most common method of oil recovery is by displacement. Typically water or a miscible gas (carbon dioxide or methane) is injected in a well (or wells) to displace oil to other wells. Ultimately the displacing fluid will break through into a production well where it must be separated from the oil. At this point, the rate of oil production decreases. For economic purposes, it is important to predict when the injected fluid will break through.

When modeling the process of oil recovery, an open question is the effect of the connectedness of the porous medium on the dynamical process of fluid displacement. If the pore space is so poorly connected as to be considered macroscopically heterogeneous, one expects the overall behavior of the flowing system to display significant anomalies. For example, it is common to investigate the physics of disordered media at a marginal state of connectivity in terms of the geometry of the spanning cluster at the percolation threshold [6, 7]. First, it is clearly an advantage to use the percolation model because a comprehensive set of exactly- and numerically-calculated critical exponents is available to describe not only its geometrical features, but also its dynamical (transport) properties. Second, the application of this geometrical paradigm can be consistently justified through “the critical path method” [8], a powerful approximation that has been successfully used [9] to estimate transport

properties (e.g., permeability and electrical conductivity) of disordered porous materials. Accordingly, the transport in disordered media with a *broad* distribution of conducting elements should be dominated by those regions where the conductances are larger than some critical value. This value is the largest conductance such that the set of conductances above this threshold forms a network that preserves the global connectivity of the system. In percolation terminology, this is equivalent to the conducting spanning cluster.

The extent to which the self-similar characteristic of the critical percolation geometry can modify the displacement process is unclear. Several studies have been devoted to the investigation of the displacement process through percolation porous media at criticality [10, 11]. More recently [12, 13], the dynamics of viscous displacement through percolation clusters has been investigated in the limiting condition of unit viscosity ratio $m \equiv \mu_1/\mu_2$, where μ_1 and μ_2 are the viscosities of the injected and displaced fluids, respectively. In this situation, the displacement front can be modeled by tracer particles following the streamlines of the flow, and the corresponding distributions of shortest path and minimal traveling time closely obey a scaling *Ansatz* [14, 15]. Subsequently [16], the dynamics of viscous penetration through two-dimensional critical percolation networks has been investigated in the limiting case of a very large viscosity ratio, $m \rightarrow \infty$. The results from this study indicate that the distribution of breakthrough time follows the same scaling behavior observed for the case $m = 1$ [12, 13]. As a consequence, it has been suggested [16] that the process of viscous displacement through critical percolation networks might constitute a single universality class, in-

dependent of m .

The spatial distributions of porosity and permeability in real rocks are often close to random. However, one cannot assume that the nature of their morphological disorder is necessarily uncorrelated, i.e, the probability for a site to be occupied is independent of the occupancy of other sites. In fact, the permeability of some rock formations can be consistently high over extended regions of space and low over others, characterizing in this way a correlated structure [3]. In the case of sandstone, for example, the permeability is not the result of an uncorrelated random process. Sand deposition by moving water or wind (and other mechanisms of geological scale) naturally imposes its own kind of correlations. A suitable mathematical approach to represent the geometry of the pore spaces and the corresponding transport properties is correlated percolation [17, 18, 19, 20, 21]. This approach has been successfully used to model permeability fluctuations and also to explain the scale dependence of hydrodynamic dispersion coefficients in real porous materials [22].

Our aim here is to extend the investigation on the displacement dynamics between two fluids through two-dimensional percolation clusters at criticality [12, 13] to the case where the pore space display long-range spatial correlations. We focus on the case of viscous penetration with two immiscible fluids of unit viscosity ratio ($m = 1$) to study the effect of long-range correlations on the distributions of traveling length and minimal traveling time.

The organization of the paper is as follows. In Section II, we present the mathematical model to simulate long-range spatial correlations and show some geometrical features of the pore structures generated by this technique. We also describe the dynamical model to simulate the process of viscous displacement in porous media. We show the results in Section III and Section IV is discussion and summary.

II. MODEL

We start by describing the geometry of the disordered system studied here. Our basic model of a porous medium is a two-dimensional site percolation cluster at criticality [6, 7] modified to introduce correlations among the occupancy units [17, 18, 19, 20, 21]. The correlations are induced by means of the Fourier filtering method (FFM), where a set of random variables $u(\mathbf{r})$ is introduced following a power-law correlation function

$$\langle u(\mathbf{r})u(\mathbf{r} + \mathbf{R}) \rangle \propto R^{-\gamma} \quad [0 < \gamma \leq 2], \quad (1)$$

where $\gamma = 2$ is the uncorrelated case and $\gamma \approx 0$ corresponds to the maximum correlation. The correlated variables $u(\mathbf{r})$ are used to define the occupancy $\zeta(\mathbf{r})$ of the sites

$$\zeta(\mathbf{r}) = \Theta[\phi - u(\mathbf{r})], \quad (2)$$

where Θ is the Heavyside function and the parameter ϕ is chosen to produce a lattice at the percolation threshold. In Figs. 1a and 1b we show typical backbones extracted from uncorrelated and correlated networks. Long-range correlations in site occupancy gives rise to variations in the structural characteristics of the conducting backbone [19]. To illustrate this effect quantitatively, Fig. 2 compares the fractal dimension of the conducting backbone calculated for uncorrelated and for correlated networks with $\gamma = 0.5$. Indeed, the fractal dimension of the backbone is significantly larger for the correlated case.

For a given correlated network at criticality, we choose two sites A and B belonging to the infinite cluster and separated by a distance r . In oil recovery these represent the injection and production wells (see Fig. 3). We then extract the percolation backbone between these two points. To model incompressible flow through this disordered system, we assume that the lattice sites have negligible volume and the allocated bonds are homogeneous elementary units of a porous material with constant permeability k and flow area a . We also consider that the dynamics of fluid displacement is governed by viscous forces and that $m = 1$ (the invading and displaced fluids have the same viscosity). Under these conditions and due to the strictly convective nature of the penetration process, the velocity at each elementary unit can be modeled in terms of Darcy's law

$$v_{ij} = \frac{k}{\mu\ell}(P_i - P_j), \quad (3)$$

where P_i and P_j are the values of pressure at sites i and j , respectively, and ℓ is the length of the bond. Conservation at each site of the backbone leads to the following set of linear algebraic equations:

$$\sum_j q_{ij} = \frac{ka}{\mu\ell} \sum_j (P_i - P_j) = 0, \quad (4)$$

where q_{ij} is the volume flow rate through the bond and the summation is taken over all bonds connected to a node i that belongs to the cluster. As a macroscopic boundary condition, we impose a constant flow rate Q between the injecting point A and the extracting point B . In practice, we apply a unit pressure drop between wells A and B , and calculate the solution of Eq. (4) in terms of the pressure field by means of a standard subroutine for sparse matrices. Due to the linearity of the system, the computed velocities at each bond, v_{ij} , can be rescaled to give a fixed total flow rate Q , independent of the distance between A and B , and the realization of the porous medium. This resembles more closely oil recovery processes where constant flow is maintained instead of constant pressure drop.

To simulate the displacement of fluid through the percolation backbone, we first note that, under the conditions of unit viscosity ratio ($m = 1$) and for a fixed pressure drop between the wells, the pressure field remains constant during the propagation of the invading front

through the percolation network. Another consequence of this simplifying assumption is that the front of invading fluid in any bond (ij) of the lattice advances locally with a constant velocity equal to v_{ij} . This situation can be expressed as

$$\frac{\partial F_{ij}}{\partial t} + v_{ij} \frac{\partial F_{ij}}{\partial x} = 0, \quad (5)$$

where $F_{ij}(x, t)$ denotes the interface between invading and displaced fluids, t is time and x corresponds to the local longitudinal coordinate within each elementary unit (bond) of the porous material. Equation (5) expresses the fact that the physical system considered here is always and everywhere convective for any value of the imposed flow rate Q . This behavior is entirely analogous to the convective (non-diffusive) regime of hydrodynamical dispersion [1, 2], where the unsteady transport of a neutral tracer in a carrier fluid flowing through a porous material is totally dominated by convective effects. In the absence of diffusive effects, the tracer samples the disordered medium by following the velocity streamlines. In the general case of hydrodynamical dispersion, however, diffusion might play a significant role. If the pore space is sufficiently heterogeneous, local zones of small velocities can be found, even under conditions of high overall flow rates. As a consequence, the propagation of the tracer front in these regions may be diffusion-like if the characteristic time for convection, $\tau_c \equiv \ell/v$, is greater than the typical diffusion time, $\tau_d \equiv \ell^2/D_m$, where D_m is the molecular diffusion coefficient of the tracer in the carrier fluid.

Applying the analogy between fluid displacement and the convective propagation of a tracer through a disordered porous material, we can now put forward a random walk picture for the front penetration of the invading fluid. Here we follow Refs. [12, 13] and use the particle-launching algorithm (PLA), where the movement of a set of (tracer) particles is statistically dictated by the local velocity field. In the PLA, each particle starting from the injection point A can travel through the medium along a different path connected to the recovery point B , taking steps of length ℓ and duration $t_{ij} = \ell/v_{ij}$ (Fig. 4). The probability p_{ij} that a tracer particle at node i selects an outgoing bond ij (a bond where $v_{ij} > 0$) is proportional to the velocity of flow on that bond, $p_{ij} \propto v_{ij} / \sum_k v_{ik}$, where the summation on k is over all outgoing bonds.

III. RESULTS

We investigate the effect of spatial long-range correlations on the distributions of traveling length and minimal traveling time. The *traveling time* t of a path \mathcal{C} is defined as the sum of the time steps t_{ij} through each bond ij belonging to a connected path between A and B

$$t \equiv \sum_{(ij) \in \mathcal{C}} t_{ij}. \quad (6)$$

The *traveling length* l is the number of bonds present in path \mathcal{C} . Among the ensemble of all paths $\{\mathcal{C}\}$, we select the path \mathcal{C}^* that has the *minimal traveling time*, t_{min} ,

$$t_{min}(\mathcal{C}^*) \equiv \min_{\{\mathcal{C}\}} t(\mathcal{C}). \quad (7)$$

This quantity corresponds to the *breakthrough time* of the displacing fluid. For a given realization of the percolation network, we compute all the traveling lengths and the minimal traveling time corresponding to the trajectories of 10 000 tracer particles. For a fixed value of r , this operation is repeated for 10 000 network realizations of size $L \times L$, where $L = 512$, so $L \gg r$. We carried out simulations for different values of r and find that there is always a well-defined region where the distributions of $P(l)$ and $P(t_{min})$ follow the scaling form [14]

$$P(z) = A_z \left(\frac{z}{z^*} \right)^{-d_z} f \left(\frac{z}{z^*} \right), \quad (8)$$

where z denotes l or t_{min} , z^* is the maximum of the probability distribution, the normalization constant is given by $A_z \sim (z^*)^{-1}$ and the scaling function has the form [12, 13]

$$f(y) = \exp(-a_z y^{-\phi_z}). \quad (9)$$

The exponents ϕ_z and d_z are related by [23]

$$\phi_z = 1/(d_z - 1). \quad (10)$$

Note that the scaling function f decreases sharply when z is smaller than z^* . The lower cutoff is due to the constraint, $l \geq r$.

In Figs. 4(a) and 5(a) we show log-log plots of the probability densities $P(l)$ and $P(t_{min})$, respectively, for five different values of “well” separation, $r = 4, 8, 16, 32$, and 64. For each curve, we determine the characteristic size z^* as the peak of the distribution and plot z^* on a double logarithmic scale. As shown in Figs. 4(b) and 5(b), the results of our simulations indicate that both l^* and t_{min}^* , respectively, have power-law dependences on the distance r , $z^* \sim r^{d_z}$. The linear fit to the data yields the exponents d_z for each distribution, namely,

$$d_l = 1.13 \pm 0.02 \quad (\text{correlated}) \quad (11)$$

and

$$d_t = 1.75 \pm 0.03 \quad (\text{correlated}). \quad (12)$$

The same exponents reported in [12, 13] for the case of flow through uncorrelated percolation networks ($\gamma = 2.0$) at constant flux are

$$d_l \approx 1.21 \quad (\text{uncorrelated}) \quad (13)$$

and

$$d_t \approx 1.33 \quad (\text{uncorrelated}). \quad (14)$$

Once more, the differences in these exponents for the correlated and uncorrelated cases can be explained in terms of the morphology of the conducting backbone. As γ decreases, the backbone becomes gradually more compact [19]. This distinctive feature of the correlated geometry tends to reduce the value of d_l and augment the value of d_t as the strength of the long-range correlations increases (i.e., γ decreases). In the limiting case of a homogeneous system, the corresponding exponents are $d_l = 1$ and $d_t = 2$ [1, 13, 24].

Figures 4(c) and 5(c) show the data collapse obtained by rescaling l and t_{min} by their characteristic size, l^* and t_{min}^* . Both scaled distributions are consistent with the scaling form of Eq. (8). From the least-square fit to the data in the scaling regions, we obtain the exponents

$$g_l = 2.35 \pm 0.05 \quad (\text{correlated}) \quad (15)$$

and

$$g_t = 1.89 \pm 0.04 \quad (\text{correlated}). \quad (16)$$

For uncorrelated pore networks subjected to the condition of constant flux, the exponents are [12, 13]

$$g_l \approx 2.0 \quad (\text{uncorrelated}) \quad (17)$$

and

$$g_t \approx 2.0 \quad (\text{uncorrelated}). \quad (18)$$

The differences between these distribution exponents have their origins in the different levels of compactness between correlated and uncorrelated clusters. These results are compatible with those of previous studies [19, 20], which indicate that spatial correlations can change other critical exponents.

IV. DISCUSSION

The need for a better description of the geometrical features of the pore space has been the main conclusion of several recent experimental and theoretical studies on transport phenomena in disordered porous materials

[3]. It is therefore necessary to examine *local* aspects of the pore space morphology and relate them to the relevant mechanisms of momentum, heat and mass transfer in order to understand the important interplay between porous structure and phenomenology. From a conceptual point of view, this task has been accomplished in many works, where computational simulations based on a detailed description of the pore space have been fairly successful in predicting and validating known correlations among transport properties of real porous media [25, 26, 27, 28, 29]. In the present work, we have investigated the dynamics of immiscible fluid displacement using the framework of a percolation model for porous media that has been specially modified to introduce spatial long-range correlations among the occupancy units of permeability. This model is certainly a more realistic description for the geometry of porous rocks and should lead to a better mathematical representation of their transport properties.

Our results on the distributions of traveling length and minimal traveling time through correlated percolation networks show that spatial fluctuations in rock permeability can have significant consequences on the dynamics of fluid displacement. More precisely, we observed that the presence of long-range correlations can substantially modify the scaling exponents of these distributions and, therefore, their universality class. As in previous studies on the subject [19, 20], we explain this change of behavior in terms of the morphological differences among uncorrelated and correlated pore spaces generated at criticality. Compared to the uncorrelated structures, the backbone clusters of the correlated cluster has a more compact geometry. The level of compactness depends, of course, on the degree of correlations introduced during the generation process. Moreover, our results are consistent with the fact that the dynamical scaling exponents d_l and d_t obtained for correlated geometries assume values intermediate between the uncorrelated and the homogeneous limiting cases.

This work has been supported by CNPq, FUNCAP, NSF, and BP-Amoco. We thank S. V. Buldyrev, N. V. Dokholyan, S. Havlin, P. R. King, Y. Lee, E. Lopez and G. Paul for helpful interactions.

[1] J. Bear, *Dynamics of Fluids in Porous Materials* (Elsevier, New York, 1972).

[2] F. A. Dullien, *Porous Media - Fluid Transport and Pore Structure* (Academic, New York, 1979).

[3] M. Sahimi, *Flow and Transport in Porous Media and Fractured Rock* (VCH, Boston, 1995).

[4] D. Ben-Avraham and S. Havlin, *Diffusion and Reactions in Fractals and Disordered Systems* (Cambridge University Press, Cambridge, 2000).

[5] P. R. King, in *North Sea Oil and Gas Reservoirs III*, ed. A. T. Buller *et al.* (Graham and Trotman, London, 1990).

[6] D. Stauffer and A. Aharony, *Introduction to Percolation Theory* (Taylor & Francis, Philadelphia, 1994).

[7] *Fractals and Disordered Systems* 2nd ed., edited by A. Bunde and S. Havlin (Springer-Verlag, New York, 1996).

[8] V. Ambegaokar, B. I. Halperin, and J. S. Langer Phys. Rev. B **4**, 2612 (1971).

[9] A. J. Katz and A. H. Thompson, Phys. Rev. B **34**, 8179 (1986); J. Geophys. Res. B **92**, 599 (1987).

[10] M. Murat and A. Aharony, Phys. Rev. Lett. **57**, 1875 (1986).

[11] J. P. Tian and K. L. Yao, Phys. Lett. A **251**, 259 (1999)

- [12] Y. Lee, J. S. Andrade, Jr., S. V. Buldyrev, N. V. Dokholyan, S. Havlin, P. R. King, G. Paul, and H. E. Stanley, Phys. Rev. E. **60**, 3425 (1999).
- [13] J. S. Andrade, Jr., S. V. Buldyrev, N. V. Dokholyan, S. Havlin, P. R. King, Y. Lee, G. Paul, and H. E. Stanley, Phys. Rev. E. **62**, 8270 (2000).
- [14] S. Havlin and D. Ben-Avraham, Adv. Phys. **36**, 695 (1987).
- [15] N. V. Dokholyan, Y. Lee, S. V. Buldyrev, S. Havlin, P. R. King, and H. E. Stanley, J. Stat. Phys. **93**, 603 (1998).
- [16] J. S. Andrade, Jr., A. D. Araújo, S. V. Buldyrev, S. Havlin, and H. E. Stanley, Phys. Rev. E. **63**, 051403 (2001).
- [17] S. Havlin, R. B. Selinger, M. Schwartz, H. E. Stanley, and A. Bunde, Phys. Rev. Lett. **61**, 1438 (1988).
- [18] S. Havlin, M. Schwartz, R. B. Selinger, A. Bunde, and H. E. Stanley, Phys. Rev. A **40**, 1717 (1989).
- [19] S. Prakash, S. Havlin, M. Schwartz, and H. E. Stanley, Phys. Rev. A. **46**, R1724 (1992).
- [20] H. A. Makse, S. Havlin, M. Schwartz, and H. E. Stanley, Phys. Rev. E. **53**, 5445 (1996).
- [21] H. A. Makse, G. Davies, S. Havlin, P.-Ch. Ivanov, P. R. King, and H. E. Stanley, Phys. Rev. E **54**, 3129 (1996).
- [22] H. A. Makse, J. S. Andrade, Jr., and H. E. Stanley, Phys. Rev. E. **61**, 583 (2000).
- [23] P. G. de Gennes, *Scaling Concepts in Polymer Physics* (Cornell University Press, Ithaca, 1979).
- [24] P. R. King, S. V. Buldyrev, N. V. Dokholyan, S. Havlin, Y. Lee, G. Paul, H. E. Stanley, and N. Vandesteeeg, Petrol. Geosci. **7**, S105 (2001).
- [25] S. Kostek, L. M. Schwartz, and D. L. Johnson, Phys. Rev. B **45**, 186 (1992).
- [26] L. M. Schwartz, N. Martys, D. P. Bentz, E. J. Garboczi, and S. Torquato, Phys. Rev. E **48**, 4584 (1993).
- [27] N. Martys, S. Torquato, and D. P. Bentz, Phys. Rev. E **50**, 403 (1994).
- [28] A. Koponen, M. Kataja, and J. Timonen, Phys. Rev. E **56**, 3319 (1997).
- [29] J. S. Andrade, Jr., M. P. Almeida, J. Mendes Filho, S. Havlin, B. Suki, and H. E. Stanley, Phys. Rev. Lett. **79**, 3901 (1997).

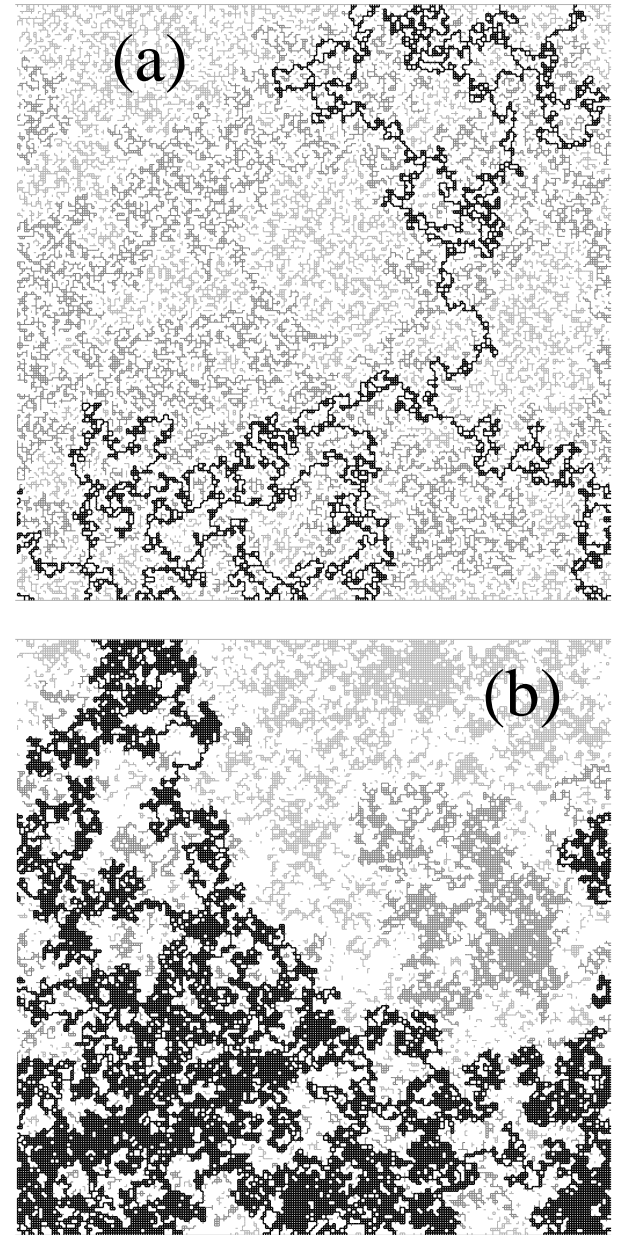


FIG. 1: (a) A typical percolation lattice $L = 256$ for the uncorrelated case. Heavy lines correspond to the backbone, gray lines to dangling ends, and light gray lines to isolated “islands” (non-spanning clusters). (b) The same as in (a), but for the correlated case ($\gamma = 0.5$).

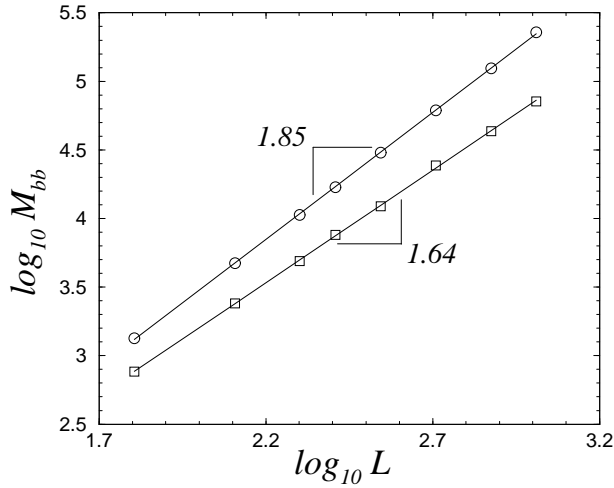


FIG. 2: Log-log plot of the backbone mass M_{bb} versus the grid size L for uncorrelated networks (squares) and correlated networks (circles). The long-range correlated percolation structures have been generated with $\gamma = 0.5$. The solid lines are the least-square fits to the data with slopes corresponding to the fractal dimensions of the respective backbones, d_{bb} .

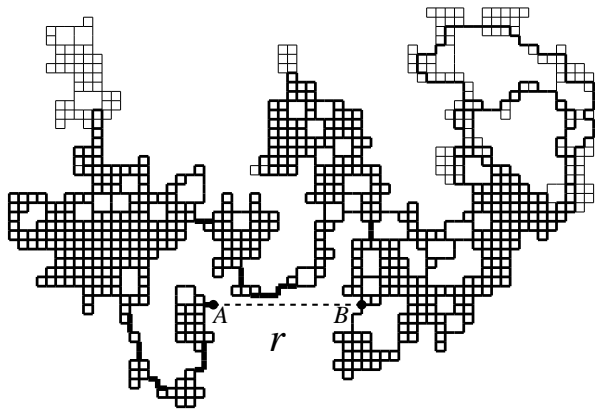


FIG. 3: The traveling paths of 10 000 tracers ($L = 64$, $r = 16$ and $\gamma = 0.5$). Heavy lines correspond to the bonds that receive more than 6000 tracers, medium lines to those that receive between 1 and 6000, and thin lines to those that receive none.

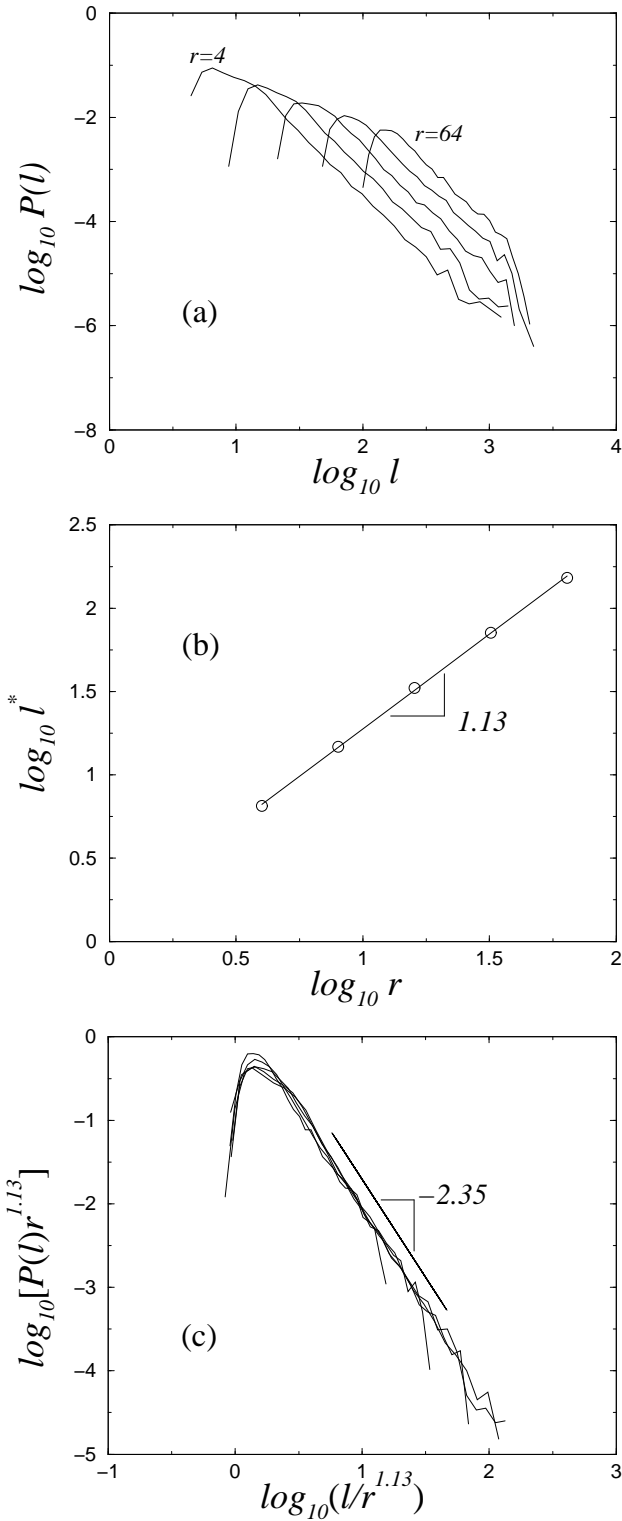


FIG. 4: (a) Log-log plot of traveling distance distribution $P(l)$ for $\gamma = 0.5$ and $r = 4, 8, 16, 32, 64$. (b) Log-log plot of the most probable value l^* for traveling length versus the distance r . The straight line is the least-squares fit to the data, $d_l = 1.13 \pm 0.02$. (c) Data collapse obtained by rescaling l with its characteristic value $l^* \sim r^{1.13}$. The least-square fit to the data in the scaling region gives $g_l = 2.35 \pm 0.05$.

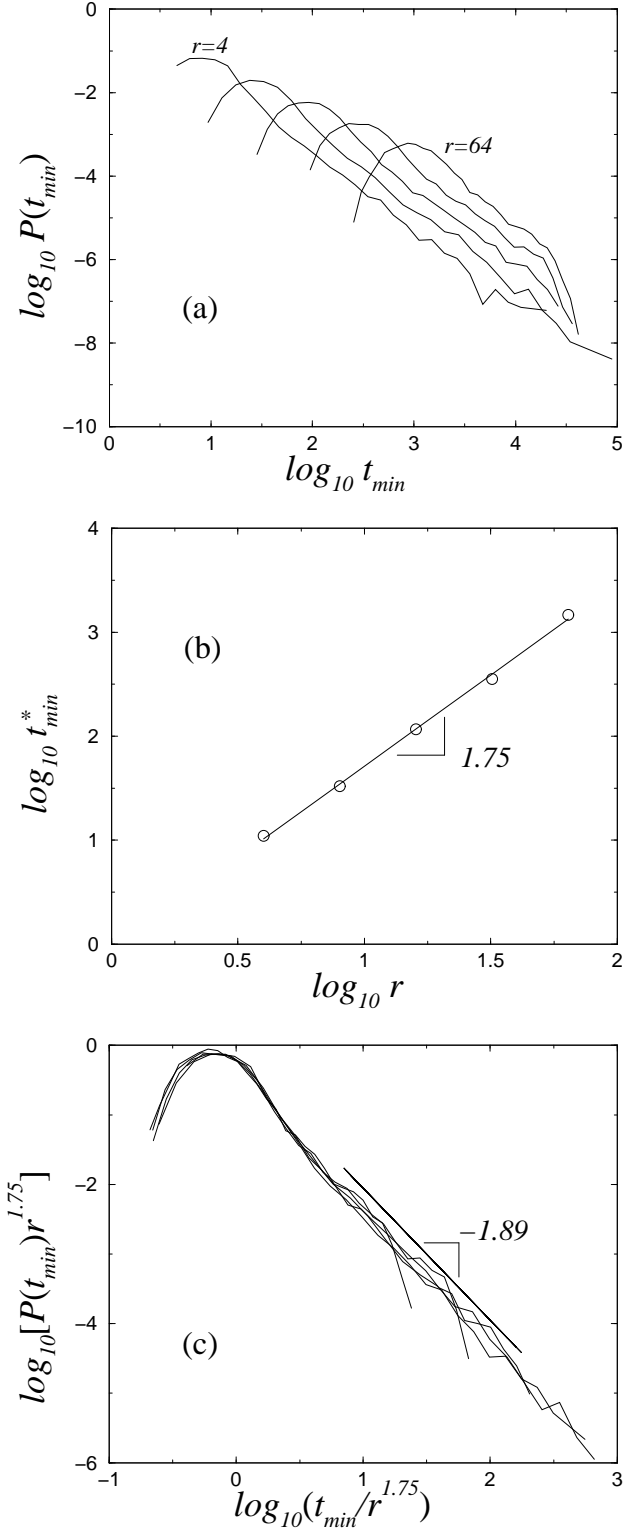


FIG. 5: (a) Log-log plot of the minimum traveling time distribution $P(t_{min})$ for $\gamma = 0.5$ and $r = 4, 8, 16, 32, 64$. (b) Log-log plot of the most probable values for the minimal traveling time t_{min} versus the distance r . The straight line is the least-square fit to the data, with the number indicating the slope, $d_t = 1.75 \pm 0.03$. (c) Data collapse obtained by rescaling t_{min} with its characteristic time $t_{min}^* \sim r^{1.75}$. The least-square fit to the data in the scaling region gives $g_t = 1.89 \pm 0.04$.